Geothermics 92 (2021) 102058

Contents lists available at ScienceDirect

Geothermics

journal homepage: www.elsevier.com/locate/geothermics

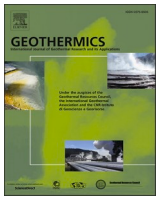

Novel computational tool for efficient structural analyses of geothermal wells

Nguyen-Hieu Hoang [a,*], Philippe Mainçon [a], David Philippe [a], Terence Coudert [a], Arve Bjørset [b], Sturla Sæther [b]

[a] Department of Materials and Nanotechnology, SINTEF Industry, Norway
[b] Equinor ASA, Arkitekt Ebbels veg 10, 7005 Trondheim, Norway

ARTICLE INFO

Keywords:
Structural modelling
Design tool
Super high temperature
Supercritical
Geothermal
Casing integrity

ABSTRACT

In geothermal energy, a huge energy potential lies in hydrothermal reservoirs close to magma where ultra-high temperature fluids (>450 °C) can be harnessed. Well casing system needs to be properly designed to ensure its integrity during its service lifetime. There currently exist neither any commonly accepted design tools nor standards regulating geothermal well design under such conditions. In this study a novel tool, Casinteg, was developed for structural analyses of geothermal wells. The tool is intended to bridge the gap between simplified analytic solutions and complex FE-based commercial software. The reliability and efficiency of the constitutive models implemented in Casinteg were verified in comparison with Abaqus. Casinteg's capability for structural analyses of full geothermal wells was preliminarily investigated, using IDDP-1 well as a case study. The calculated stress in the production casing was in a good agreement between Casinteg and Ansys models, while the computational time of Casinteg simulations was within minutes. Further developments are still needed. However, preliminary results were encouraging and have demonstrated the benefit of Casinteg for efficient structural analyses of full geothermal wells.

1. Introduction

The world is currently facing a growing need for energy. To answer this need and at the same time fighting against the global climate change, diversified and sustainable energy sources are indispensable. The lower demand for oil and the increasing demand for alternative sources of energy from wind, solar, and geothermal energy is presently seen as a mega trend for green shift in energy use. Among the renewable energy, geothermal energy is today recognized as a weather independent and stable energy source with significant potential compared to other resources. Evidently, geothermal energy has a high initial cost related to exploration and reservoir mapping and thereby high upfront risk. Even so, successful geothermal projects have a lower levelized cost of electricity (LCOE) than some solar and wind energy projects. High enthalpy geothermal systems have been harnessed for electrical power generation for over several decades. To date, most developed geothermal systems have temperatures in the order of 150–300 °C, and they are considered to be able to provide high enthalpy fluids (Axelsson and Gunnlaugsson, 2000; Hochstein, 1990; Benderitter and Cormy, 1990; Muffler and Cataldi, 1978). The LCOE of geothermal energy can be lowered by hunting and producing electrical power from super-critical fluid reservoirs (temperature about 450–550 °C and pressure up to 300 bars). In these conditions, the geothermal fluid has a much higher enthalpy ($\geq$ 2900kJ/kg) than steam and liquid extracted with conventional geothermal wells, thus potentially multiplying the electricity output by a factor of 5–10 and hence lowering the LCOE of geothermal projects.

However, the aggressive fluids and high temperatures encountered in these geothermal reservoirs are tough challenges for the well materials and structures when the operation lifetime is at least 20 years. The casing system, which is a composite structure with steel casing string and cement sheath on its outside, needs to be designed to ensure the integrity of the geothermal well, and to protect the shallow environment against contamination, under the expected harsh conditions. Low-cost and robust casing systems are absolute requirements for any geothermal well to minimize the LCOE. However, it is a tough challenge to achieve, especially for the super High Temperature (HT) condition. During their lifetimes, casing systems are subjected to cyclic thermo-mechanical loads, which can increase the failure risk. Experiences

* Corresponding author.
E-mail address: hieu.nguyen.hoang@sintef.no (N.-H. Hoang).

https://doi.org/10.1016/j.geothermics.2021.102058
Received 27 April 2020; Received in revised form 27 January 2021; Accepted 2 February 2021
Available online 8 February 2021

Nomenclature

$\boldsymbol{\sigma}, \sigma_{\mathrm{VM}}, \sigma_y$	Cauchy stress tensor, equivalent von-Mises stress and flow stress
$\boldsymbol{\varepsilon}, \boldsymbol{\varepsilon}_e, \boldsymbol{\varepsilon}_p, \boldsymbol{\varepsilon}_\tau, \boldsymbol{\varepsilon}_c$	Tensors of total strain, elastic strain, plastic strain, thermal strain and creep strain
λ_r, λ_s	Normal stress and shear stress
$\mu, \lambda_{\max}$	Coulomb friction coefficient, and shear cutt-off
σ_0, A, n	Yield stress and power law parameters for strain hardening
τ, t	Temperature and time
C, D, α	Heat specific, thermal conductivity and thermal expansion coefficient of materials
E, ν, K, G	Young modulus, Poisson's ration, bulk and shear moduli
K, m	Norton creep parameters
r, θ, z	Radial, hoop and axial direction in cylindrical coordinate system
u_r, u_θ, u_z	Corresponding displacements

have shown that the casing may fail by (a) mechanical buckling, (b) tensile failure (in threaded connection or cross section), (c) hydrogen embrittlement, and (d) corrosion, see Fig. 1 for illustration. In other words, improper materials selection and design may lead to serious failure events, and loss of the production well (Snyder, 1979; Southon, 2005; Kruszewski and Wittig, 2018), as already happened in the past Icelandic Deep Drilling Project No. 1 (IDDP-1).

As discussed, the challenges to achieve a robust casing construction for super HT geothermal power plants are mostly related to material technologies (to develop and select casing, sealant materials and couplings) and to the lack of standards regulating the geothermal well design practices for such operation temperature. New Zealand Standard, NZS 2403 (NZSN, 2015), the most commonly used reference for geothermal well design, covers solely the design condition up to 350 °C, which is much lower than the temperature at hand for supercritical fluids. To arrive at a robust casing construction in such conditions, novel solution strategies other than the conventional geothermal construction ones are required. Developing these strategies requires collaboration of a number of industrial and R&D actors who together provide an understanding of the complex challenges, and sufficient research and innovation capability. Several drilling attempts and R&D projects have been carried out all over the world, searching for identifying the technology gaps, solving the related common challenges to bring the supercritical geothermal power in real use (Reinsch et al., 2017). Among which are cited the drilling projects IDDP-1 and recently IDDP-2 (Elders and Friðleifsson, 2010), together with the synergy European projects H2020-GeoWell (Ragnarsson et al., 2018) and H2020-DeepEGS (Friðleifsson et al., 2019).

In order to evaluate the technological viability of alternative design solutions, systematic researches combining experimental tests, numerical model development and design tools are needed. Analytic/semi-analytic solutions are conventionally used as efficient tools to design O&G and geothermal casing systems (ANSI, 2008; Rahman and Chilingarian, 1995). However, these analytic/semi-analytic models are often developed based on simplified considerations of boundary conditions, material and joint behaviour, and geometrical configurations. These models can hardly be applicable for super-HT casing system design where cyclic thermo-mechanical loads, non-linearity in properties of involved materials, inhomogeneity in well geometry are present. Recently, Kaldal et al. (2016) have demonstrated successful uses of the commercial Finite Element (FE) based code Ansys to understand the mechanical response of the full well IDDP-1 under thermo-mechanical loading, while accounting for the complexity of its load history, plasticity and temperature dependent properties of casing materials. Their results depicted that commercial FE-based software can theoretically be used to analyze the stress in the casing system, thus supporting the well design and the well operation planning. However, FE model-based design of full geothermal wells leads to practical issues when it comes to engineering applications due to its complexity of inputs management and its costly computational time. A typical full well simulation may take days or even weeks in terms of computational time. It is also to note that in Kaldal's models the creep behaviour of casing in super high temperature conditions, was not taken into account. Accounting for the casing creep behaviour in the model may eventually pile up the numerical complexity and computational time.

To overcome the discussed drawbacks encountered both in analytic models and in FE-based models with commercial software, more user-friendly and efficient computational tools are needed both for better understanding down-hole physics and for designing robust casing systems of geothermal wells. In view of that, a novel and stand-alone non-linear Finite Element based software, Casinteg, is developed in the context of HotCaSe project, which is led by Equinor and backed up by the Research Council of Norway (ENERGIX Programme) (Hoang et al., 2020; Gruben et al., 2021). The present paper aims at providing a brief theory introduction to element formulation, heat transfer, contact and material models implemented in Casinteg (Section 2). A preliminary verification of the implemented constitutive models was carried out through a comparison with the commercial Abaqus software based on well segment models (Section 3). Finally, the performance of Casinteg to analyze the full well was investigated and demonstrated. Models of IDDP-1 well were established in Casinteg and the corresponding

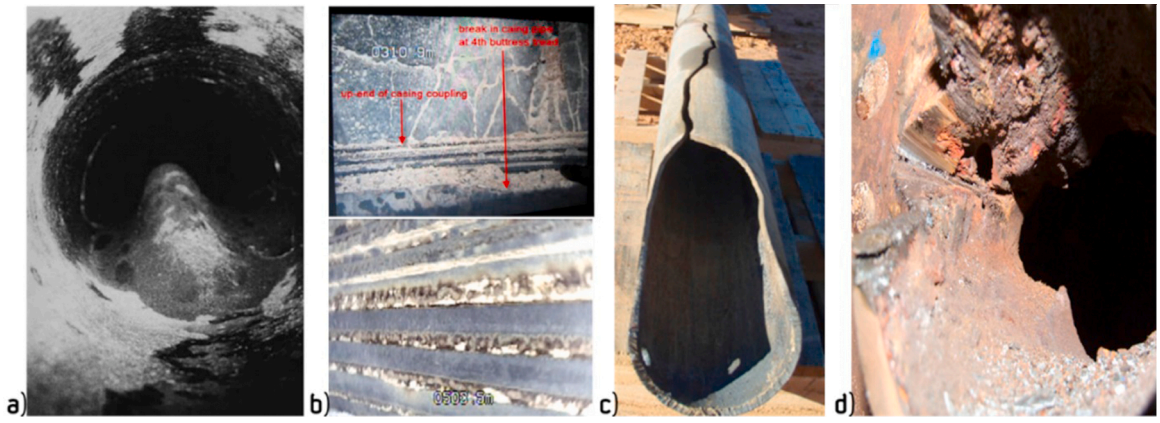

Fig. 1. Failure modes in casing: (a) Casing implosion/buckling, (b) tensile failure in threaded pipe joint, (c) hydrogen embrittlement and (d) corrosion (Thorbjornsson, 2016).

analyses results were compared with the results obtained by Ansys models as presented in Kaldal et al. (2016) (Section 4).

2. Theory of computational tool – Casinteg

Casinteg is a Finite Element (FE) based software adapted for structural analyses of the global behaviour of wells, with an emphasis on geothermal wells. The present section aims at providing a brief introduction to the theory of element formulation, heat transfer, contact and material models implemented in Casinteg, together with its assumptions and hypotheses. Related limitations of the current Casinteg version are also discussed, paving path for further possible developments of the tool.

2.1. Assumption and numerical solving scheme

2.1.1. Assumption

Fig. 2a shows a typical schematic geometry of conventional geothermal wells, where the annuli are cemented up to surface to maintain negligible axial displacement of the casing under thermo-mechanical loadings during operations. As seen, from a geometric perspective the well structure seems to be "axisymmetric", constituting of steel pipes and cement and formation layers.

To simplify the problem and develop a numerical model that can be efficiently solved with sufficiently reasonable accuracy, the following assumptions were made:

- The structure is assumed to be geometrically axisymmetric. Any effects of dogleg deviation, asymmetry due to cementing are not represented. In view of this assumption, the cylindrical coordinate system is used in Casinteg with r the radial coordinate, z the axial coordinate, θ the hoop or circumferential coordinate as illustrated in Fig. 2b. The corresponding displacements are noted u_r, u_z and u_θ respectively.
- Geometries, loads and numerical solutions are θ-independent (cylindrical symmetry) and there is no rotation in the circumferential direction ($u_\theta = 0$).
- Heat transfer in the axial direction along the well depth is not considered. Only the transfer in the radial direction is accounted for and modelled. Changes in temperature and pressure in the wellbore hole along the well depth are accounted for as loading input parameters to Casinteg models.
- The well depth is significantly larger than the well diameter. As an implication, the shear stress and deformation in the axial direction in the casing and cement are assumed to be negligible as compared with other components. Thus, shear deformation ε_{zr} in the continuum materials is not studied. On the contrary, the shear component at the interfacial contact is important, and any shear induced by shear friction/slip at the contact interfaces is accounted for by enforcing the equilibrium with the axial stress through the thickness of continuum elements.
- The problem is assumed to be static and any dynamic related problems, e.g. influences of the acceleration, wave propagation are not considered. As a consequence, only the first order derivatives of degrees of freedom are to be accounted for in the differential equations.

2.1.2. Numerical solving scheme

Casinteg is coded using Julia programming language (Bezanson et al., 2017). Julia is a relatively young language, but presenting many advantages facilitating the implementation of an efficient calculation tool, e.g. its flexibility and possibility to connect with other languages, a high performance of automatic differentiation algorithms. Casinteg models are solved using the implicit numerical solving scheme of the differential equations.

(1) Backward Euler method:

Let $\bar{x}$ stand for a set of degrees of freedom in general for the whole model and t for time. Assuming that the equilibrium of the structure at any time can be represented by a set of non-linear differential equations of the following form

$$\bar{f}\left(\bar{x}, \dot{\bar{x}}, t\right) = \bar{0} \tag{1}$$

Assuming also that the solution $\bar{x}_{k-1}$ at time step t_{k-1} is known, the implicit solving method consists of finding the equilibrium state at time step t_k with $\bar{x}_k$ as unknown. The above Eq. (1) can be re-written with the following Euler's backward approximation:

$$\bar{f}\left(\bar{x}_k, \frac{\bar{x}_k - \bar{x}_{k-1}}{t_k - t_{k-1}}, t_k\right) = \bar{0} \quad \text{or} \quad \bar{f}(\bar{x}_k, (\bar{x}_k - \bar{x}_{k-1})\beta, t_k) = \bar{0} \tag{2}$$

in which

$$\beta = \frac{1}{t_k - t_{k-1}} \tag{3}$$

Eq. (2) can be solved using the Newton-Raphson method.

(2) Newton-Raphson iterations:

The Newton-Raphson iteration method consists of finding the solution $\bar{x}_k^{i+1}$ of the non-linear equation Eq. (2) at iteration $i+1$, knowing the solution $\bar{x}_k^i$ at iteration i, using the following equation:

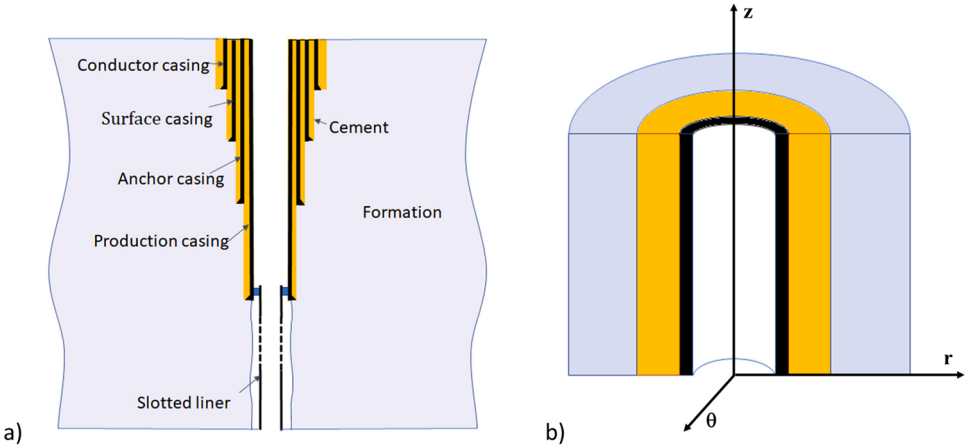

Fig. 2. (a) Typical schematic geometry of conventional geothermal well and (b) representative cylindrical coordinate system in Casinteg.

$$\overline{x}_k^{i+1} = \overline{x}_k^i - \frac{\overline{f}\left(\overline{x}_k^i\right)}{\overline{f}'\left(\overline{x}_k^i\right)} \tag{4}$$

The iterative procedure is repeated until the condition $||\overline{f}\left(\overline{x}_k^{i+1}\right)|| \leq$ tolerance is reached.

(3) Automatic differentiation:

In the above equation Eq. (4), the differentiation term of $\overline{f}'\left(\overline{x}_k^i\right)$ appears. Automatic differentiation algorithms are made possible in Julia by overloading floats with dual numbers, providing the accurate differential value of $\overline{f}'$ at $\overline{x}_k^i$. This is remarkably fast, even for an element with high degrees of freedom, it takes only twice as long to compute the element imbalance force vector and stiffness matrix as it takes to compute the imbalance force vector alone (Bezanson et al., 2017).

2.2. Constitutive models

2.2.1. Continuum element modelling

Owing to the axisymmetric assumption, 2D axisymmetric elements are used to discretize the structure of the geothermal wells. As discussed, shear deformations are not considered in the continuum material element for the problem at hands. In a well, frictional forces at the contact interfaces play a significant role. However, the displacements (e.g. within the thickness of a steel casing) related to this shear deformation are very small (micrometers) compared to the vertical displacements that a casing may experience (meter). As a consequence, the traditional approach of rectangular elements with displacement and rotation degrees of freedom (DoF) attached to nodes at the corners would not be necessary and would result in poor numerical solutions. In addition, the well length is significantly larger than the diameter of the casing. Using conventional elements would require a fine discretization of the well geometry along the axial direction to maintain a reasonable aspect ratio. An excessive mesh refinement in axial direction certainly results to a high computational time, as observed with commercial FE codes.

To overcome these drawbacks of the conventional elements, simplified 2D axisymmetric elements were proposed to represent the continuum materials in the well structure modelled in Casinteg, as illustrated in Fig. 3a. As seen, the elements are modelled by four nodes located in the middle edges, which are different from the conventional elements where the nodes are located at their corners. In addition, the simplified elements have reduced degree of freedoms (DoF), e.g. two radial displacement DoF r_{DoF} attributed to the two nodes representing the radial position of the elements, two axial displacement DoFs z_{DoF} attributed to the two nodes representing their axial position. No rotation DoFs are needed. Furthermore, two temperature DoFs τ_{DoF} are used to model the radial heat transfer through the elements. Since the heat transfer along the well depth is neglected, the temperature DoF in the axial direction is not needed. In total, six DoFs are used for each element, as seen in Fig. 3a. To these DoFs correspond the four linear shape functions:

$$\begin{aligned} N_1(r) &= \frac{r_o - r}{r_o - r_i}, \quad N_2(r) = \frac{r - r_i}{r_o - r_i} \\ N_3(z) &= \frac{z_t - z}{z_t - z_b}, \quad N_4(z) = \frac{z - z_b}{z_t - z_b} \end{aligned} \tag{5}$$

in which o, i, t, b denote the spatial position of the element nodes, respectively corresponding to the outer, inner, top and bottom positions. The element has one reduced integration Gauss point located at its centre.

2.2.2. Heat transfer modelling

As discussed, only heat transfer in the radial direction is considered in Casinteg. The heat transfer is modelled based on the thermal conduction using the second Fick's law, which is written as:

$$C\dot{\tau} + \overline{\nabla}\cdot\overline{J} = 0 \tag{6}$$

with

$$\overline{J} = -D\overline{\nabla}\tau \tag{7}$$

Here, C and D are respectively the heat specific and thermal conductivity of materials. We seek an approximate solution to this differential equation, of the form

$$\tau(r,t) = \sum_i N_i(r)\tau_i(t) \tag{8}$$

in which, $N_i(r)$ are linear shapes functions for radial direction as shown in Eq. (5). The differential equation is enforced in a weak formulation:

$$\forall i \quad \int_v N_i(C\dot{\tau} - D\overline{\nabla}\cdot\overline{\nabla}\tau)\mathrm{dv} = 0 \tag{9}$$

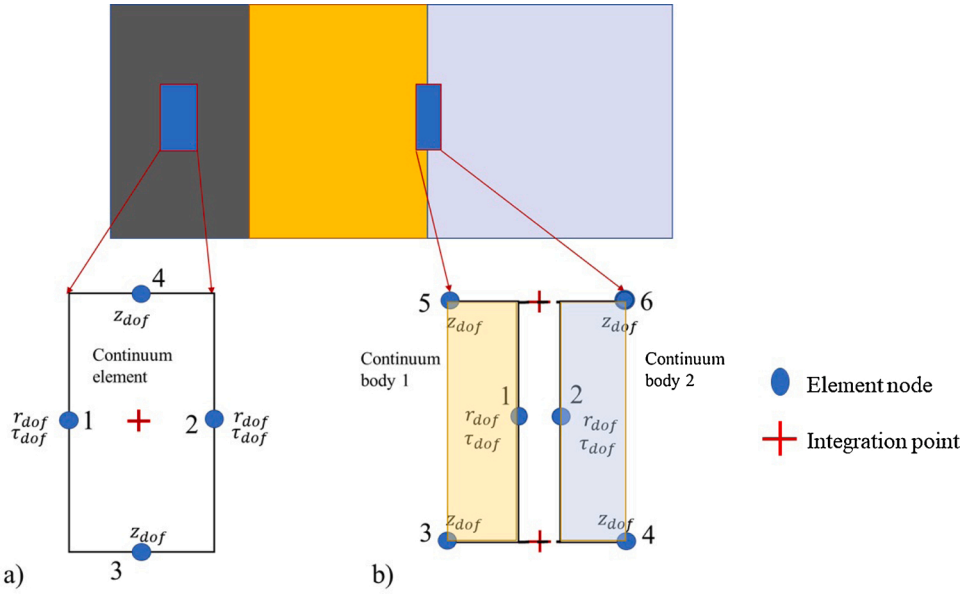

Fig. 3. Illustration of elements implemented in Casinteg. (a) Continuum element, and (b) gap element.

Using partial integration, this becomes:

$$\forall i \quad \sum_j \int_v N_i \mathrm{CN}_j \mathrm{d}v \dot{\tau}_j - \sum_j \int_v \overline{\nabla} N_i \cdot D \overline{\nabla} N_j \mathrm{d}v \tau_j + \int_s N_i \mathrm{J} \mathrm{d}s = 0 \tag{10}$$

Considering a vertical length L of element, in the absence of heat flow in the z direction:

$$\forall i \quad \sum_j \left[\int_{r_i}^{r_o} N_i \mathrm{CN}_j \ 2\pi \mathrm{r} \mathrm{L} \mathrm{d}r \right] \dot{\tau}_j - \sum_j \left[\int_{r_i}^{r_o} \overline{\nabla} N_i \cdot D \overline{\nabla} N_j 2\pi \mathrm{r} \mathrm{L} \mathrm{d}r \right] \tau_j - N_i(r_o) J(r_o) 2\pi r_o L + N_i(r_i) J(r_i) 2\pi r_i L \quad = 0 \tag{11}$$

The heat capacity expression $\int_{r_i}^{r_o} N_i \mathrm{CN}_j \ 2\pi \mathrm{r} \mathrm{L} \mathrm{d}r$ in Eq. (11) is of the 3rd degree in r, requiring a 2nd order Gauss scheme for integration.

2.2.3. Contact modelling

The contact between two continuum bodies needs to be modelled properly in order to be able to enforce the equilibrium of the axial forces (z-direction), considering the possible shear forces present at the interfaces due to friction, in spite of no shear deformations/stresses accounted for in the solid continuum elements. In order to handle the interfacial behaviour precisely and efficiently, the contact between two continuum bodies is modelled using special gap elements implemented in Casinteg, see Fig. 3b, instead of using interaction based models between two surfaces (or set of nodes) as in the commercial software. As seen, the spatial description of gap elements is modelled by six nodes shared with the two neighbouring continuum elements, i.e. three nodes on the left and three on the the right side of the contact interface, respectively.

The gap element requires the radial displacements u_{r1}, u_{r2} and temperature τ_{r1}, τ_{r2} at the left and right of the gap (at nodes 1 and 2) as inputs. In addition, the axial displacements u_{z1}, u_{z2} at the left and right bottom (or top) nodes shared with continuum elements (nodes 3, 4 for bottom nodes and nodes 5, 6 for top) are also required as inputs to compute the interfacial sliding behaviour. Two integration points are attributed accordingly to the bottom and top of the elements to calculate the contact stresses corresponding to the relative displacement between u_{z1}, u_{z2}. The normal and shear stresses at the contact interfaces, denoted as λr and λs respectively, are solved as extra DoFs to the equilibrium equation systems, using the inequality contact constraint and Coulomb friction constitutive model as discussed below.

(12) Inequality constraints and contact detection.:

Let's $\delta u_r = u_{r1} - u_{r2}$ and $\delta u_z = u_{z1} - u_{z2}$ be the relative radial and axial displacements, respectively. δu_r and δu_z can in a more general way be expressed as:

$$\delta u_r = L_r \bar{x}, \quad \delta u_z = L_z \bar{x} \tag{12}$$

in which $\bar{x}$ is the set of degree of freedoms of the whole model. For the contact problem, the following inequality constraint needs to satisfied:

$$\delta u_r = L_r \bar{x} \geq 0 \tag{13}$$

If there is contact, the constraint $\delta u_r = L_r \bar{x} = 0$ is enforced to the equilibrium condition of the whole system. Using the Lagrange multiplier method, the optimal equilibrium solution under such constraint is obtained by solving the following equation:

$$\begin{cases} \bar{f}(\bar{x}) + \lambda_r \nabla_{\bar{x}} (L_r \bar{x}) = \bar{f}(\bar{x}) + \lambda_r L_r = 0 \\ L_r \bar{x} = 0 \end{cases} \tag{14}$$

where $\bar{f}(\bar{x})$ is the differential equation for the equilibrium solution of the structure, and λ_r is the Lagrangian multiplier, physically representing the contact stress (negative if compressive). In case of no contact detected, the constraint is inactive. Knowing the equilibrium at time step t_{k-1}, and the incremental external load ΔR between time steps t_{k-1} and t_k, iterative calculations predict trial values of $\bar{x}_k$ and $\lambda_{r,k}$. A corrector operation is applied in the gap elements to enforce the inequality constraint in Eq. (13) using Eq. (14)

(13) Coulomb friction model.:

Since the rate dependency and dynamic effects are not considered in Casinteg, the standard Coulomb friction model was implemented. The model assumes that no relative motion occurs if the equivalent frictional stress λ_s is less than the critical stress which is proportional to the contact pressure λ_r and friction coefficient μ.

$$\|\lambda_s\| \geq \lambda_{\text{critic}} = \mu \|\lambda_r\| \tag{15}$$

A cut-off value $\lambda_{\max}$ is also introduced to the friction model to put the limit on the shear stress:

$$\lambda_{\text{critic}} = \min(\mu \|\lambda_r\|, \lambda_{\max}) \tag{16}$$

Given a predicted value $\bar{x}_k$ at time t_k, the trial elastic shear stress can be expressed as:

$$\lambda_{s,k}^{\text{trial}} = k_s \left(\delta u_{z,k} - \delta u_{z,k-1} \right) \tag{17}$$

In which k_s is the shear stiffness, while $\delta u_{x,k} = L_z \bar{x}_k$ and $\delta u_{x,k-1} = L_z \bar{x}_{k-1}$ are respectively the relative axial displacement between two sides of contact at time steps t_k and t_{k-1}. When the trial elastic shear traction is equal to or greater than the shear limit, i.e. $\left\| \lambda_{s,k}^{\text{trial}} \right\| \geq \|\lambda_{\text{critic}}\|$, sliding between two interfaces occurs. Otherwise, the contact is "elastically stuck". In case sliding is detected, the shear stress is constraint to be equal the shear limit.

2.2.4. Material modelling

For geothermal wells, the casing may be expected to thermally yield under extreme temperature operation loading, thus a strain-based design approach may be required. Standards New Zealand, NZS 2403 NZSN (2015) refers to seminal work by Holliday (1969), and to Canadian Industry Recommended Practice 03 (Drilling, 2012), but provides no quantitative basis for the application of post-yield design. In addition, it is to be noted that the Holliday approach does not account for any possible stress relaxation due to creep (viscous) behavior of casing materials that could occur above 200 °C (NZSN, 2015). To increase the flexibility in super-HT casing design, three material models, namely Thermo-Elastic, Thermo-Plastic, and Thermo-Plastic-Creep, were implemented in Casinteg accounting for the temperature dependency of elastic properties (Young's modulus, Poisson's ratio), plastic properties (yield stress and work hardening), and creep properties.

The main ingredients of the model are a yield criterion, an isotropic thermal expansion, an associated flow rule with a nonlinear isotropic strain-hardening rule, and a Norton-like creep law.

The strain tensor $\boldsymbol{\varepsilon}$ is assumed to be additionally decomposed into thermal, elastic and plastic and creep parts:

$$\boldsymbol{\varepsilon} = \boldsymbol{\varepsilon}_{\boldsymbol{\tau}} + \boldsymbol{\varepsilon}_e + \boldsymbol{\varepsilon}_p + \boldsymbol{\varepsilon}_c \tag{18}$$

where $\boldsymbol{\varepsilon}_{\boldsymbol{\tau}}$, $\boldsymbol{\varepsilon}_e$, $\boldsymbol{\varepsilon}_p$ and $\boldsymbol{\varepsilon}_c$ are respectively the thermal, elastic, plastic and creep strain tensors. The relation between the Cauchy stress tensor and strain is defined as:

$$\boldsymbol{\sigma} = \mathrm{C} : \boldsymbol{\varepsilon}_e = \mathrm{C} : \left(\boldsymbol{\varepsilon} - \boldsymbol{\varepsilon}_e - \boldsymbol{\varepsilon}_p - \boldsymbol{\varepsilon}_c \right) \tag{19}$$

where **C** is the fourth-order tensor of the elastic constants. For isotropic elastic materials as assumed in the present work, the Cauchy stress tensor can also be expressed as:

$$\boldsymbol{\sigma} = 3\mathrm{K}\ \mathrm{vol}(\boldsymbol{\varepsilon}_e) + 2\mathrm{G}\ \mathrm{dev}(\boldsymbol{\varepsilon}_e) \tag{20}$$

where K and G are respectively the bulk and shear moduli as a function of temperature τ, which are related to the Young's modulus E and Poisson's ratio ν by:

$$K(\tau) = \frac{E(\tau)}{3(1-2\nu(\tau))}, \quad G(\tau) = \frac{E(\tau)}{2(1+\nu(\tau))} \tag{21}$$

Assuming isotropic thermal expansion, the thermal strain tensor can be calculated by:

$$\boldsymbol{\varepsilon}_\tau = \alpha \Delta\tau \boldsymbol{I} \tag{22}$$

in which α is the thermal expansion coefficient, $\Delta\tau$ is the temperature change, and $\boldsymbol{I}$ the unit tensor. The plasticity is modelled using von-Mises yield criterion with isotropic strain hardening. The yield function f which defines the elastic domain in stress space, is expressed as:

$$f = f(\boldsymbol{\sigma}) - \sigma_Y = \sigma_{\mathrm{VM}} - \sigma_Y \leq 0 \tag{23}$$

in which σ_{VM} is the equivalent von-Mises stress and σ_Y is the follow stress. The latter is modelled with the hardening power constitutive law as follows:

$$\sigma_Y = \sigma_0(\tau) + A(\tau)\overline{\varepsilon_p}^{n(\tau)} \tag{24}$$

where $\overline{\varepsilon_p}$ is the equivalent plastic strain, while $\sigma_0(T)$, $A(T)$ and $n(T)$ are material parameters defining the temperature dependent yield stress and strain hardening, respectively. In this constitutive model, it is assumed that the plastification of materials is completely separated from the creep mechanisms. This assumption implies that the creep strain does not have any contribution to the strain hardening of materials.

The associated flow rule defines the evolution of the plastic strain tensor and the equivalent plastic strain as:

$$\dot{\boldsymbol{\varepsilon}_p} = \dot{\overline{\varepsilon_p}}\frac{\partial f}{\partial \boldsymbol{\sigma}} = \frac{3}{2}\dot{\overline{\varepsilon_p}}\frac{\mathrm{S}}{\sigma_{\mathrm{VM}}} \tag{25}$$

where S is the deviatoric part of the Cauchy stress tensor $\boldsymbol{\sigma}$.

In this present work, only the secondary creep is accounted for in the model and the creep strain rate tensor is defined by the following creep flow rule:

$$\dot{\boldsymbol{\varepsilon}_c} = \dot{\overline{\varepsilon_c}}\frac{\partial f}{\partial \boldsymbol{\sigma}} = \frac{3}{2}\dot{\overline{\varepsilon_c}}\frac{\mathrm{S}}{\sigma_{\mathrm{VM}}} \tag{26}$$

with $\dot{\varepsilon_c}$ being the steady creep rate defined by the following Norton-like power law:

$$\dot{\overline{\varepsilon_c}} = K(\tau)\left(\frac{\sigma_{\mathrm{VM}}}{\sigma_0(\tau)}\right)^{m(\tau)} \tag{27}$$

In Eq. (27), $K(\tau)$ and $m(\tau)$ are material parameters defining the temperature dependency of secondary creep behaviour. It is to note that owing to the stress normalization, $m(\tau)$ is dimensionless while $K(\tau)$ is a time dependent parameter.

2.3. Discussion – current limitations and further development

Casinteg was developed based on certain simplification hypotheses, which are necessary for an efficient computational tool. The simplifications may not lower the predictive accuracy of Casinteg models, as compared with the similar models established in other commercial FE-based software as shown in the next sections. However, the simplifications for efficiency trade-off may lead to some limitations in modelling complex geometries. Owing to the axisymmetric assumptions in Casinteg, non-axisymmectric problems, e.g. casing stand-off and well deviation, cannot be assessed directly. An adequate modelling strategy could be, however, adopted to assess the risks related to each problem. For instance, simulations with various cement sheath thicknesses could be performed together with probabilistic-based analyses to evaluate the risks associated to the casing stand-off. Also, as the bending and shear stresses of the casing cannot be captured under the axisymmetric assumption with the simplified continuum elements, Casinteg could not be used to design the well of high dogleg severity. Development of a more advanced continuum element may be needed in further works to better model highly deviated wells.

For the same sake of efficiency, the casing joints are not represented in Casinteg full well models. Consequently, some local information at the coupling locations cannot be captured in the full well analyses. The anchoring effect due to the coupling geometry, which globally constrains the relative axial displacement between the casing strings and the cement sheath, could be modelled by the bonding contact at the casing/cement interface in the present study. However, this simplification is not fully representative to the real physics in the well, where possible micro-annuli at the casing/cement interfaces might be created due to the cyclic temperature and pressure loads. The combination of the joint anchoring effect and the interfacial debonding mechanism at micro-annuli creation cannot be simulated neither by the bonding contact nor the sliding contact model. In further work of the authors, a miscellaneous interfacial model will be developed and implemented for that purpose.

In addition, the current model library implemented in Casinteg was mainly developed for casing materials. The possibility to simulate the behaviour of the well cement and formation materials is currently still rather limited. In this first Casinteg version, only the thermo-elastic model is available for these materials, describing the temperature dependency of their elastic properties (i.e. Young's modulus, Poisson's ratio). This means that creep and others poro-mechanical behaviour of these materials, e.g. pressure dependency, permanent compaction due to pore collapse under pressure, possible pore pressure build-up at HT could not be simulated. A more advanced poro-mechanical material model is needed to investigate the impact of these cement and formation behaviours on the casing strings in the super hot geothermal well.

Bearing in mind that Casinteg should be adapted for structural analyses of the global well behaviour, stresses in the casing systems after the well completion should be taken into account as the initial conditions prior to the structural analyses. The initial stress in the casing strings resulting from the installation (i.e. the tensile stress under its self-weight in a well filled with drilling fluid) can be modelled by applying the gravity load with a buoyancy factor to the casings. To account for the cementing effect, the cement slurry prior to the setting time is modelled as liquid. The stress in the cement slurry prior to setting can be expressed in terms of the slurry density ρ_s, the specific gravity g and the cement depth location z as follows:

$$\boldsymbol{\sigma} = -\rho_s g z \boldsymbol{I} \tag{28}$$

In the present work, the cement hydration effect is not modelled and the isochoric cement hydration is assumed. This assumption implies that any possible cement shrinkage/swelling during the hydration process is not considered, and the hydraulic stress in the cement slurry is transferred as the initial stresses applied to the casing strings when the cement is set. In reality, any cement volumetric change due to the hydration process would alter the resulting stresses on the casing strings (Saint-Marc et al., 2020; Bois et al., 2012). Thus, neglecting the hydration effect may impact the final stress results in the analysed casing systems. Further development is necessary to account for the cement hydration and analyse its effect on the casing integrity.

The stress state in the formation due to gravity and drilling operations is also an important aspect. The formation stresses after drilling, when being properly modelled as initial conditions to a poro-mechanical

material model, may have an impact on the structural response of the casing systems. However, in the present study the formation is modelled by a Thermo-Elastic material model, where the poro-mechanical behaviour and failure mechanisms of the formation are not subjects for investigation. In view of that, the formation stresses after drilling could be neglected in the subsequent simulations.

Also note that in the current Casinteg version, the pressure and temperature in the wellbore along the well depth (i.e. axial direction) are given as the loading inputs, which are directly applied to the inner surface of the innermost casing string at different well life events. The temperature evolution due to the heat conduction in the radial direction of the whole well structure is subsequently calculated using constitutive equations implemented in Section 2.2.2. An integrated wellbore thermic predictor allowing for the computation of the temperature and pressure changes in the wellbore could also be an important further development, ensuring a more reliable and more efficient design of geothermal casing systems.

3. Verification – well segment modelling

This current section aims to provide a preliminary verification of the constitutive models, namely heat transfer, casing material models, contact model implemented in Casinteg. This was done by benchmarking with the commercial software Abaqus. It is to note that the main objective here is to verify the constitutive models. Thus, it is not necessary to perform full well analyses. Models of simple well segments of 12m length (of order of the casing segment length) were used for efficiency reasons. The performance of Casinteg for analyzing full geothermal wells is demonstrated in Section 4.

3.1. Model description

Three models of 12m long well segments, consisting of multi-layers of casing, cement and formation, were established in Casinteg, see Fig. 4 for illustration. The three models have respectively one, two and four casing string layers, representing well segments at different well depths of the full well illustrated in Fig. 2. All the casing strings were 12mm thick, while the cement sheath thickness is determined by the casing geometry and drill bit geometry as shown in Table 1. In all the models, the rock radius was chosen to be 5m. The model geometry is summarized in Table 1.

The three well segments were modelled using respectively 5200 elements, 6400 elements and 8800 elements, in which three elements through thickness and two hundred elements in axial direction were used for casing strings, see Fig. 4d for illustration of the model mesh. The studied casing is a typical API casing, namely L80, and modelled by constitutive material model described in Section 2.2.4. Cement sheath and formation were instead modelled as thermo-elastic materials. The bottom and top of the whole model were constrained in u_z displacement, except for the production casing string (i.e. the innermost casing) where the top was free to move axially under thermal loading. In all the three models, the radial displacement, u_r, of the end rock was constrained, see Fig. 4 for illustration.

Table 1
Casing geometry and cement sheath for well segment models.

Casing	Casing thickness (mm)	Casing OD (inch)	Drill bit OD (inch)
Conductor casing	12	22:5	26
Surface casing	12	18:625	21
Anchor casing	12	13:575	17:5
Production casing	12	9:635	12:25

The initial stresses in the established well segment models were set to zero, neglecting any effect of the well drilling/completion. This is acceptable in this study, bearing in mind that the main objective here is to verify the constitutive models. The initial temperature in the whole models was set homogeneously at 50 °C. A cyclic temperature load, ramping from 50 °C to 500 °C during one day, staying constant at 500 °C for thousand days then cooling down to the initial temperature 50 °C, was applied to the inner surface of the innermost casing, see Fig. 5.

The mechanical response of the three casing segments under this

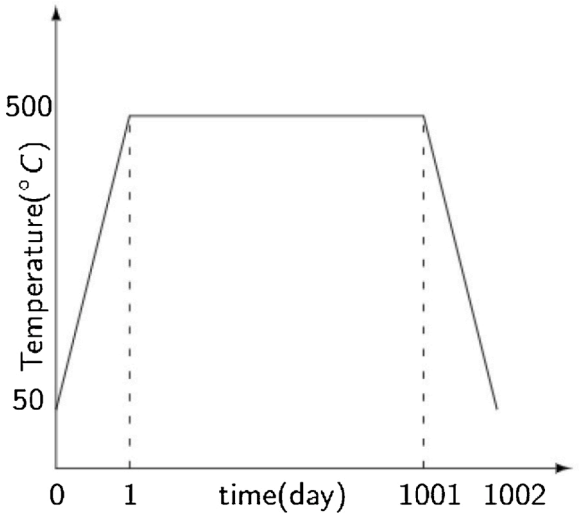

Fig. 5. Thermal load profile.

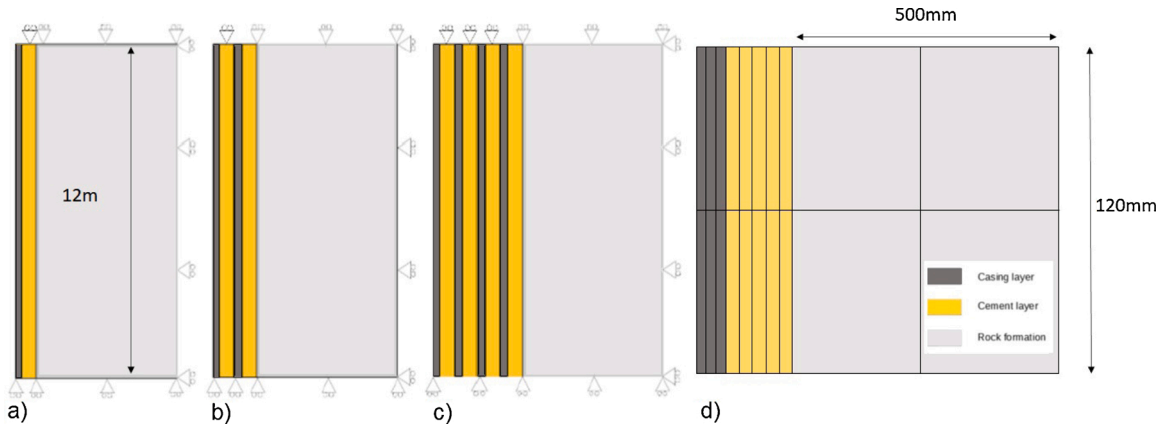

Fig. 4. Multi-layers casing segment models: (a) One casing string model, (b) two casing string model, (c) four casing string model, and (d) illustration of the model mesh showing 3 and 5 elements of casing and cement layers in the radial direction.

thermal load was investigated and compared with the results obtained with the same models generated in Abaqus. For both Casinteg and Abaqus models, the thermo-elastic and plastic properties of L80 casing material were taken from Kaldal et al. (2015). Due to the lack of creep data, general creep properties were generated for L80 steel. It is to keep in mind that the main objective of this study is to benchmark constitutive models implemented in Casinteg with Abaqus. Thus, the experimental data of L80 steel is not of importance as long as the same creep properties were used in the both models. The final model parameters describing the L80 material behaviour are then summarized in Table 2. The material properties for cement and formation were also taken from Kaldal et al. (2015) and summarized in Table 3.

3.2. Results and discussion

3.2.1. Base case study

In this Section, results of the base case simulations of Casinteg are presented and discussed in regard with the Abaqus simulations. In the base case study, creep behaviour of casings was not accounted for and only thermo-elastic-plastic constitutive parts of the material model were considered in both Casinteg and Abaqus. The contact between different parts (i.e. casing, cement and formation) was modelled as perfect bonding (i.e. no relative axial sliding at contact interface was considered). In addition, a perfect thermal conductivity at the contact interface was assumed, meaning that no heat loss can occur due to heat transfer through the contact interface.

Fig. 6 shows the comparison of the temperature evolution as a function of time in different layers of the well segments. Note that the plotted results were taken from the middle of each layer thickness. It can be seen that the temperature in casing and cement layers predicted by Casinteg was in a very good agreement with the Abaqus results. The percentage difference in temperature in casing and cement layers between Casinteg and Abaqus at the end of each phases, namely warm-up, operation and cool-down, was calculated and recapitulated in Table 4 for the first segment model (i.e. one casing string). The percentage difference is defined as $||200(\mathrm{res}_{\mathrm{Casinteg}} - \mathrm{res}_{\mathrm{Abaqus}})/(\mathrm{res}_{\mathrm{Casinteg}} + \mathrm{res}_{\mathrm{Abaqus}})||$, in which $\mathrm{res}_{\mathrm{Casinteg}}$ and $\mathrm{res}_{\mathrm{Abaqus}}$ are respectively the numerical results obtained from Casinteg and Abaqus. As can be seen, the highest difference was observed in cement layer. However, the accumulated difference after multiple loading phases (end of cooling) is not significant between the two codes. The results depicted that the heat transfer model by conductivity implemented in Casinteg is reliable for modelling the geothermal wells.

The mechanical response under this temperature load, in terms of stress and strains in the casing layers of three segment models, are shown in Fig. 7. A very good comparison of Casinteg and Abaqus's results was observed in the three segment models, both for axial stress, von-Mises stress and plastic deformation. The obtained results with the two codes are almost identical in most of the cases. A slight difference was, to some extent, found for plastic deformation. This is probably due to the fact that in Casinteg the plastic strain hardening was modelled by power law as in Eq. (24), while in Abaqus the stress-strain relation was accounted for by interpolation using piecewise tabulated values. In any case, the accumulated percentage difference was insignificant, as documented in Table 5 for the one casing string segment model. It is also interesting to note that the plastic deformation in the first casing (i.e. production casing) decreases with increasing numbers of casing strings/cement layers in the models, even though the temperature change experienced by the production casing is the same for all models. This is because the apparent radial stiffness around the production casing decreases with increasing cement thickness in multi-layers models, which in turns affects the triaxial von-Mises stress and the plastic deformation.

Table 2
L80-steel and K55-steel properties.

Temperature (°C)	20		350		500	
Steel	L80	K55	L80	K55	L80	K55
Young Modulus (GPa)	217	205	183	171	163	129
Thermal expansion (10^{-5}/K)	12		12:5		13:5	
σ_0 (MPa)	634	390	454	290	350	250
A (MPa)	2002	1065	807	819	449	720
n	0:91	0:62	0:39	0:49	0:30	0:42
K (1/hour)	1:78E − 95		7:85E − 5		1:37E − 4	
m	6:66		6:6		6:6	
Specific heat (J/kg/K)	400	490	400	490	400	490
Thermal conductivity (W/m/K)	50:4	50	50:4	50	50:4	50
Poisson's ratio	0:3					
Density (kg/m^3)	7800					

Table 3
Cement and rock properties.

	Cement	Rock
Young Modulus (GPa)	2:4	80
Thermal expansion (10^6/K)	10	5:4
Poisson's ratio	0:15	0:31
Density (kg/m^3)	1600	2650
Specific heat (J/kg/K)	880	840
Thermal conductivity (W/m/K)	0:81	2

3.2.2. Influence of material models

Fig. 8 illustrates the effect of the three implemented material models, namely Thermo-Elastic, Thermo-Plastic and Thermo-Plastic-Creep, on the casing stress evolution in the first casing segment model (i.e. one casing string model). It can be seen that modelling the casing as a Thermo-Elastic material significantly overshot the actual stress in the casing. It is crucial to account for the thermo-plastic behavior during the warm-up, allowing for the strain-based design of the casing. On the other hand, the creep behavior governing the stress relaxation in the casing under constant strain, is of importance to be considered when dealing with cyclic loading, e.g. during the well cool-down. It can be seen that due to stress relaxation at the constant operating temperature during the production time, the calculated tensile stress in the casing when cooled down is significantly higher than that obtained with other models. The high tensile is a main driving force for tensile failure in the HT geothermal casing when cooled down for maintenance, as for example IDDP-1 well. The results thus depicted that the casing's creep behavior cannot be neglected for a reliable design of geothermal wells, especially in in super-HT conditions.

The previous section has demonstrated the reliability of the Thermo-Plastic model implemented in Casinteg. In this section, Thermo-Plastic-Creep model is verified in comparison with the constitutive model implemented in Abaqus (Hibbitt et al., 2012). The verification study was done by using the one-casing string segment model as shown in Fig. 4a. The comparison results are given in Fig. 9. It can be seen that the stresses in the casing obtained by Casinteg and Abaqus are almost identical. However, the predicted plastic strain by Casinteg is somewhat higher than the Abaqus result. This is probably because the creep deformation in Casinteg is assumed not to contribute to plastic strain hardening, which is not the case in Abaqus. The contribution of the creep deformation to the work hardening as assumed in Abaqus results in an increased material strength, and consequently lowering the plastic deformation under the same loading, see Fig. 9c. Experimental tests are needed to provide a better understanding of the involved creep mechanisms, and verify the assumption behind the creep model theory. Still the creep model implemented in Casinteg can be used with a great confidence for evaluating the stress in geothermal casings, while the calculated plastic deformation is on the conservative side for design purposes.

3.2.3. Influence of Coulomb friction contact model

The previous study was done with the bonded interfacial behaviour

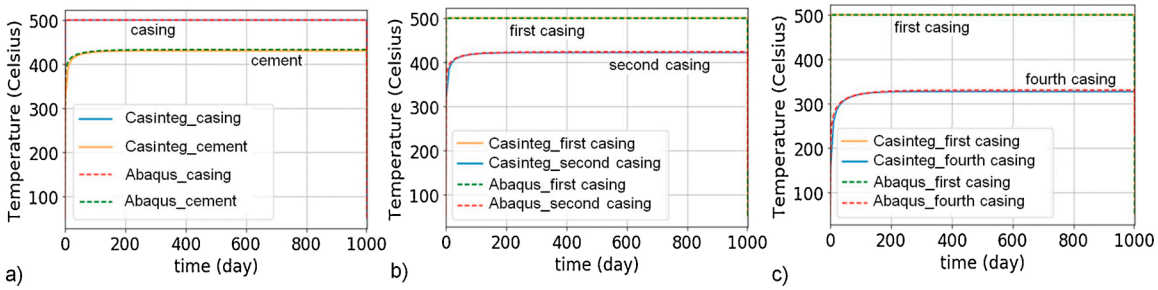

Fig. 6. Comparison of temperature results from Casing and Abaqus in different parts of the well for the three segments in Fig. 4, (a) one-casing segment, (b) two-casing segment, and (c) four-casing segment. The dashed lines are results from Abaqus, and the full lines are from Casinteg.

Table 4
Temperature comparison between Casinteg and Abaqus for one casing segment model.

Time/Temperature (C)	End warming	End production	End cooling
Abaqus_Casing	499.4	499.8	50.3
Casinteg_Casing	499.4	499.8	50.4
DIFFERENCE (%)	0.006	0.001	0.059
Abaqus_Cement	332.9	432.4	149.9
Casinteg_Cement	319.8	430.2	160.4
DIFFERENCE (%)	3.934	0.497	6.546

at all the contact interfaces, meaning that no axial relative displacement between layers was allowed. In this section, the Coulomb friction model was used to investigate the sliding contact behaviour. The friction coefficient was set equal to 0.1, which may not be realistic for the frictional behaviour between casing and cement. However, the real value is not important in this benchmarking study as long as the same coefficient was applied in both Castinteg and Abaqus models. The other parameters were kept unchanged, and the Thermo-Plastic model was used for the casing as for the base case study.

Fig. 10 shows the Casinteg simulation results in terms of axial stress, von-Mises and plastic strain taken out from the elements at the middle casing layers for the three models illustrated in Fig. 4. The Casinteg results are plotted along with the corresponding Abaqus ones.

It can be seen that the results obtained with both the Casinteg and Abaqus models in this study are very comparable. The stress and strain results in the first casing (innermost casing) of these models somewhat lower than the ones with the bonding contact shown in Fig. 7, especially for the two and four casing segment models. This is because the casing slides to some extent against the cement under the temperature load at hands, thus releasing the developed thermal stress in the casing, and consequently lowering the plastic deformation. However, the casing is not totally free to slide, but held back by the friction force.

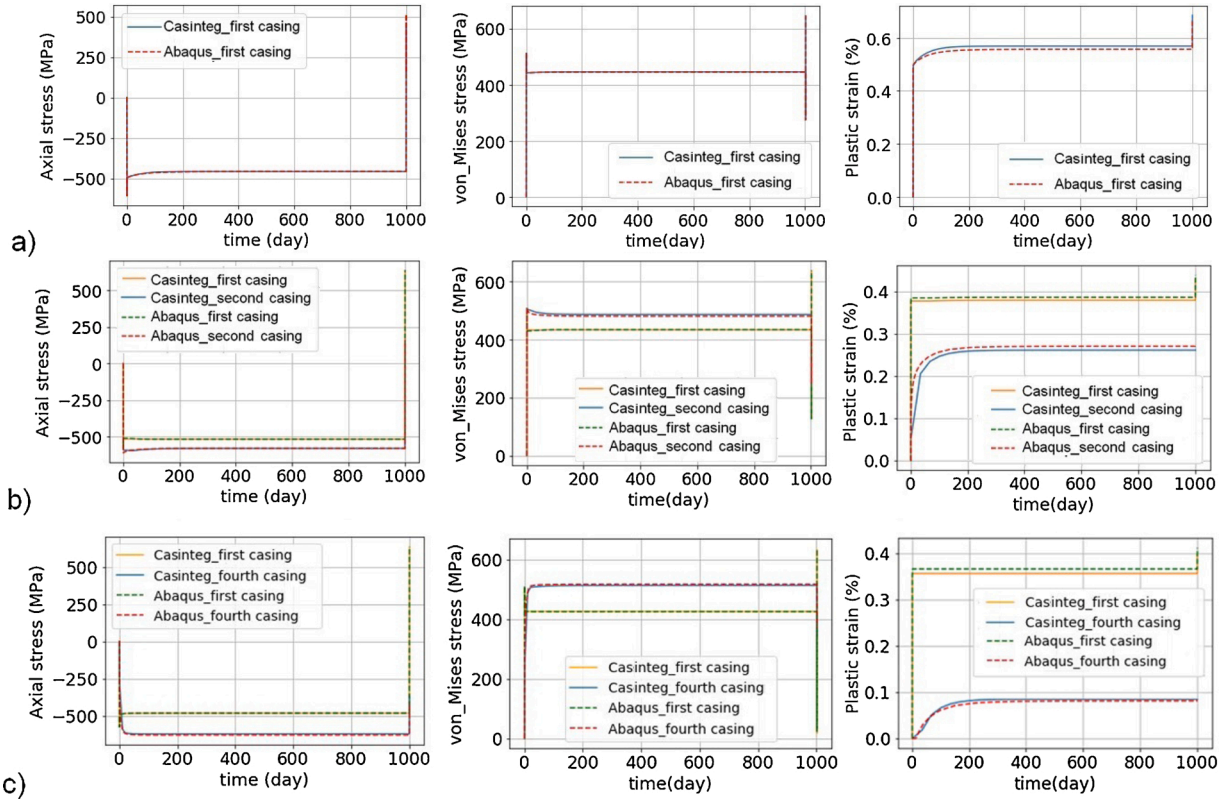

Fig. 7. Comparison of stress and strain in casings between Abaqus/Casinteg models for base case study (Thermo-Plastic material for casing and bonding interactions between layers) for the three segments: (a) One casing segment model, (b) two casing segment model, and (c) four casing segment models. The dashed lines are results from Abaqus, and the full lines are from Casinteg.

Table 5
Percentage differences in stress and plastic strain results between Casinteg and Abaqus for the one-casing segment model (base case study with Thermo-Plastic material and bonding contact).

	End warming	End production	End cooling
Time/Axial stress (MPa)			
Abaqus	−498.0	−459.0	648.0
Casinteg	−497.0	−455.0	667.0
DIFFERENCE (%)	0.326	0.905	2.958
Time/Von Mises stress (MPa)			
Abaqus	443.0	446.0	648.0
Casinteg	442.0	445.0	643.0
DIFFERENCE (%)	0.155	0.098	0.751
Time/Plastic strain (%)			
Abaqus	0.473	0.541	0.666
Casinteg	0.495	0.569	0.685
DIFFERENCE (%)	4.749	5.14	2.843

3.3. Preliminary discussion

The benchmarking study in the previous sections showed a very good agreement between Casinteg and Abaqus results for all the investigated models. This study validated the reliability of the constitutive models implemented in Casinteg, ensuring the confidence in using the developed tool for geothermal well analyses. However, it is to note that the core advantage of Casinteg is its efficiency in terms of the computational time. With exactly the same models, it is about ten time faster to perform simulations in Casinteg than in Abaqus. The remarkably lower computational time in Casinteg is mainly due to the reduced degree of freedoms of the implemented elements and the automatic differentiation method made available in Julia (Bezanson et al., 2017). The computational efficiency of Casinteg can even be significantly increased by increasing the mesh size in the models, since the Casinteg result is less mesh dependent in comparison with the other FE-based commercial software, as discussed in the mesh sensitivity study in Section 4.

4. Thermo-mechanical modelling of full geothermal well

Despite the efficiency and accuracy of Casinteg in modelling well segments shown in the preceding, the modelling of full wells of thousands meter length may be more computational demanding. In this Section, the performance and efficiency of Casinteg for structural analyses of full geothermal wells were investigated and demonstrated. Models of IDDP-1 well were established in Casinteg and their analyses results were compared with the corresponding Ansys results presented in Kaldal et al. (2016).

4.1. Mesh sensitivity

To select an optimal mesh size while still ensuring the accuracy of the Casinteg numerical results for full well simulations, the mesh sensitivity study was performed in this section, using the one-casing segment model shown in Fig. 4a. In this study, the modelled well segment was thousand meter long, instead of twelve meter as in the previous sections, allowing for the investigation of coarser mesh sizes. The element number through casing thickness was kept unchanged, i.e. three elements, while the element sizes in the axial direction varied from one meter to five hundred meters to investigate the effect of element aspect ratios. The latter is defined as the ratio of the largest to the smallest sides of the element. The API Carbon Steel K55, which was the main casing grade in the IDDP-1 well, was also used for the casing in this mesh sensitivity study. The material data for K55 were taken out from Kaldal et al. (2015) and summarized in Table 2. The cement and rock materials were the same as in the previous study and their properties were given in Table 3. The same boundary condition and temperature loading shown in Fig. 5 were applied to the investigated model, and only the bonding contact model was considered in this study. Fig. 11 shows the results in terms the axial stress, von-Mises stress and plastic deformation taken out from the middle element of the casing with different model mesh sizes. It depicted that the Casinteg results are not sensitive to the mesh size. Solution convergence, both for the stresses and plastic strain, was obtained even with a large element of two hundred meter length, corresponding to an extreme element aspect ratio of 50000 in this case. The solution convergence is better confirmed in Fig. 12, showing a zoom of the Fig. 11 at the transition time from the end of warm-up to the constant operation temperature. It is to note that for the conventional elements as in the commercial software Abaqus, an aspect ratio of maximum three is recommended for reasonable numerical solutions. The large aspect ratio would lead to a shear locking pathology, consequently poor numerical

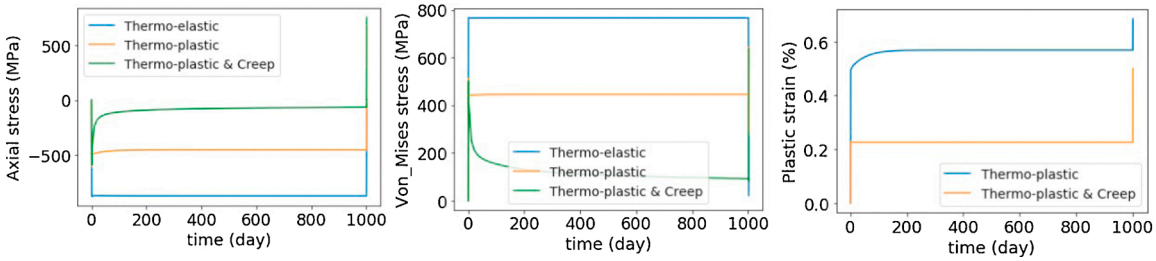

Fig. 8. Effect of the used material models on the predicted stress-strain evolution in the casing.

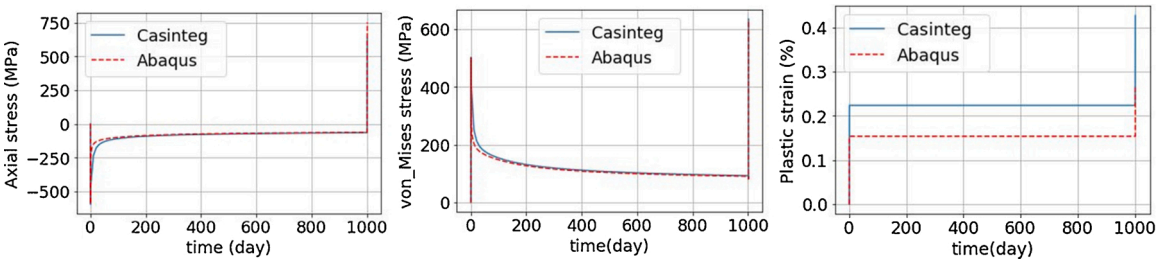

Fig. 9. Comparison between Casinteg and Abaqus results for the one-casing segment model with Thermo-Plastic-Creep material and bonding contact: (a) Axial stress, (b) von-Mises stress and (c) plastic deformation.

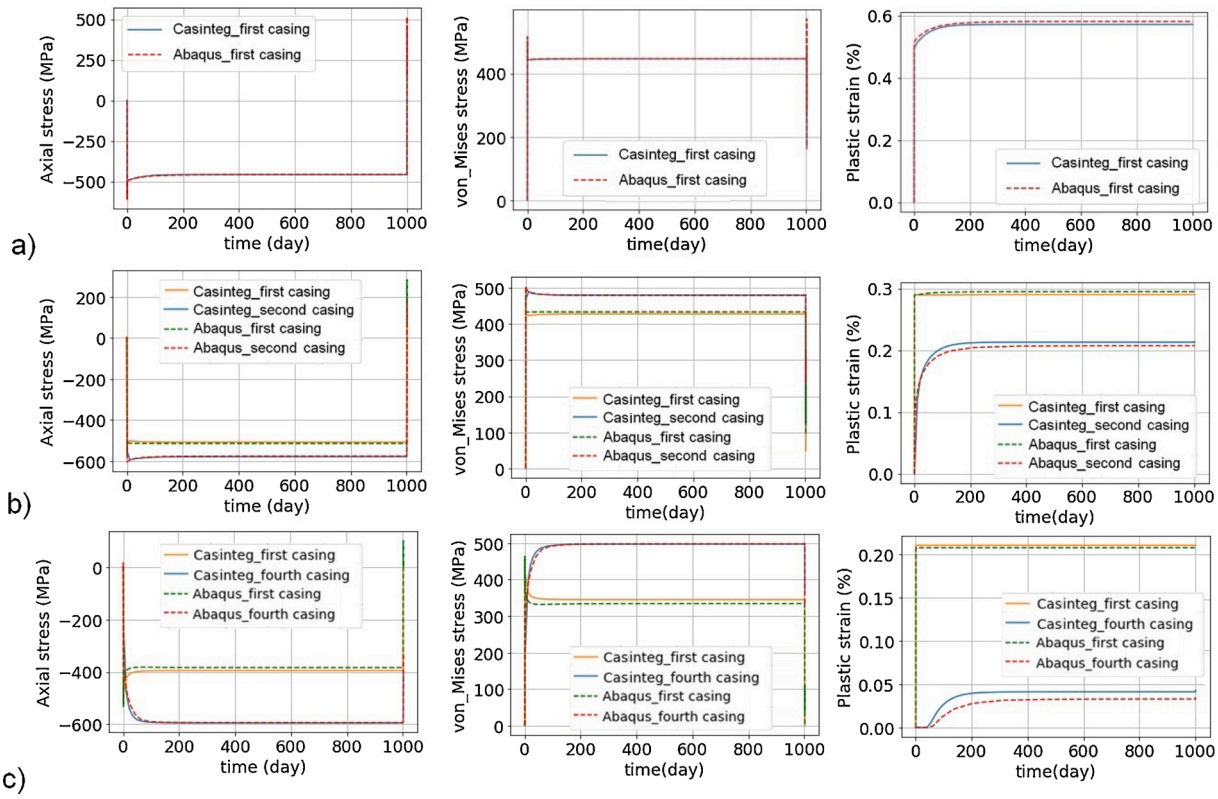

Fig. 10. Comparison of stress and strain in casings between Abaqus/Casinteg models (Thermo-Plastic material for casing and sliding interactions between layers) for the three segments: (a) One casing segment model, (b) two casing segment models, and (c) four casing segment models. The dashed lines are results from Abaqus, and the full lines are from Casinteg.

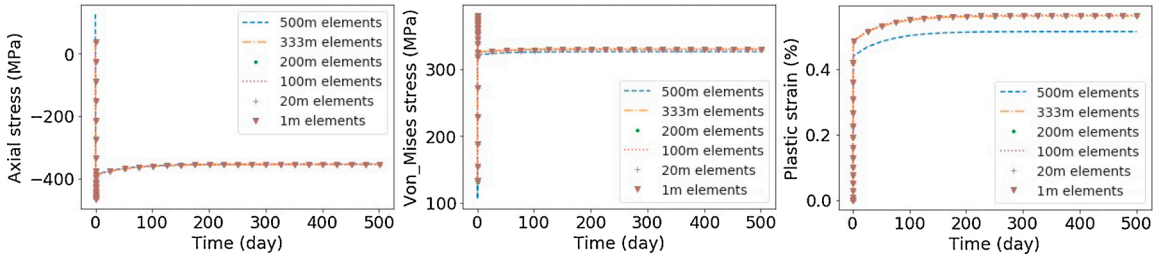

Fig. 11. Evolution of axial stress, von-Mises stress and plastic strain for different meshes.

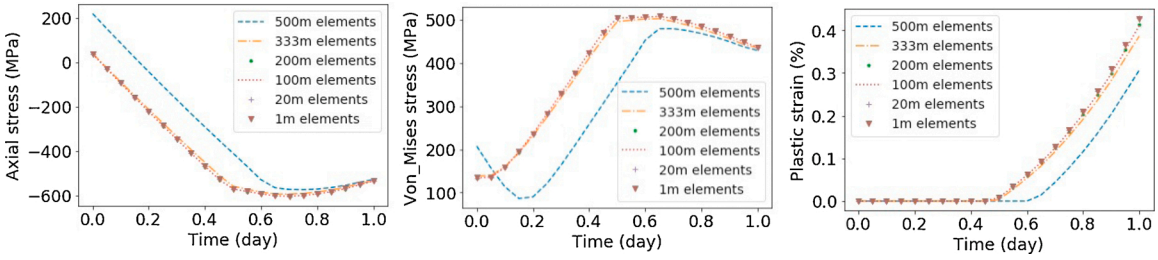

Fig. 12. Zoom of Fig. 11 during the first day.

results (Zienkiewicz and Taylor, 2005). In Casinteg, the implemented continuum element has no rotational degree of freedoms, and limited DoFs in displacement. This hinders the possibility for Casinteg to handle problems in which the shear stresses cannot be neglected. However, it is to remind that the special continuum element in Casinteg was implemented under the assumptions stated in Section 2.1, in which the bending and shear stresses are neglected. Owing to its simplicity, the shear locking is avoided for Casinteg element, rendering the numerical results much less mesh dependent.

4.2. *Modelling of IDDP-1 well*

To investigate the performance of the developed tool for structural analyses of full geothermal wells, numerical models of IDDP-1 well were

established in Casinteg. Simulations of IDDP-1 through its relevant loading history were carried out and the obtained results were compared with the Ansys ones presented by Kaldal et al. (2016).

The IDDP-1 well geometry is illustrated in Fig. 13a (Friðleifsson et al., 2015). The model of IDDP-1 established in Casinteg had the same geometry as used by Kaldal et al. (2016), which is summarized in Table 6. The readers are referred to Kaldal et al. (2016) for more information of the IDDP-1 well model in Ansys.

As discussed in the sensitivity study, a mesh size of hundred meters in the axial direction was selected in this study for optimal solution, while three, five and twenty elements were respectively used for casing and cement and rock layers in the radial direction. Note that casing and cement layers were described with a regular mesh; while the rock is radially meshed with a bias ratio of 100 toward the end of model, see Fig. 13b for illustration. The casings were modelled as thermo-plastic materials as in the Ansys model, except for the surface casing X56 for which only the thermo-elastic behaviour was adopted. The cement and formation layers were also modelled as thermo-elastic materials. All the material properties are summarized in Table 2 and Table 3 for casing and cement, rock materials respectively. To account for the anchoring effects of the casing couplings in the well, the bonding contact was used to model the interfacial behaviour at all the contact interfaces.

The loading history in terms of temperature and pressures profiles applied to the IDDP-1 well is shown in Fig. 14. As seen, six loading phases, namely the initial cementing phase and discharge phases from I to V, were reported and accounted for in Casinteg simulations. The formation temperature profile was applied at the outer rock to simulate the far-field temperature. The IDDP-1 well was actually going through various shut-in periods in between the discharge loads prior to its end-of-life quenching by cold water, see Fig. 15 for illustration (Kaldal et al., 2016). However, due to the lack of information about these temperature load profiles, the shut-in phases were neglected in the Casinteg models.

In order to account for the initial condition in the well prior to any thermo-mechanical load in the well bore, the cementing temperature profile (see Fig. 14) was applied to the production casing inner surface at the beginning of the simulations. A steady state simulation was first run to set the initial temperature to the whole model. In addition, initial stresses in the casing resulted from the installation (i.e. tensile stress from a casing hanging free from the top in a well filled with drilling fluid) were accounted for by applying the gravity load with a buoyancy factor of 0.78 to the casing before the cement setting. Also note that the cement hydration effect was not modelled in the present work. Isochoric cement hydration was assumed in all the simulations, and the hydraulic pressure of cement slurry was taken as initial stress state in the set cement for structural analyses. Neglecting the hydration effect and possible cement compaction behaviour due to pore collapse may have significant impact on the stress evolution in casing systems. However, this is considered out of scope of the current study.

Table 6
Casing geometry of IDDP-1 well model.

Casing layer	Diameter (in)	Thickness (mm)	Length (m)	Steel grade
Surface casing	32 1/2	13:0	87	X56
Intermediate casing 1	24 1/2	13:0	254	K55
Intermediate casing 2	18 5/8	13:0	785	K55
Anchor casing	13 3/8	13:1	1939	K55
Production casing	9 5/8	13:8	1949	K55

An effort was made to duplicate as much as possible the same conditions for IDDP-1 simulation in Ansys as in Casinteg. However, due to the different nature of the two codes, the same model of IDDP-1 with exactly the same boundary conditions and material models in Ansys could not be replicated in Casinteg. Also note that the cement Young's modulus reduction as a function of temperature was not considered in the Casinteg model as in the Ansys ones due to uncertainties in the cement property reported by Kaldal et al. (2016, 2015). In these works, a Young's modulus of 2.4 GPa was documented for the cement, but unclear at which temperature. However, it is to keep in mind that the main objective of this study is to demonstrate the performance and efficiency of Casinteg for modelling the full geothermal well while considering the complicated loading history. Thus, a perfect comparison between Ansys and Casinteg models would not be necessary.

4.3. Results and discussion

Fig. 16 shows the comparison between Ansys and Casinteg simulations of IDDP-1 well in terms of axial stress along the well depth at

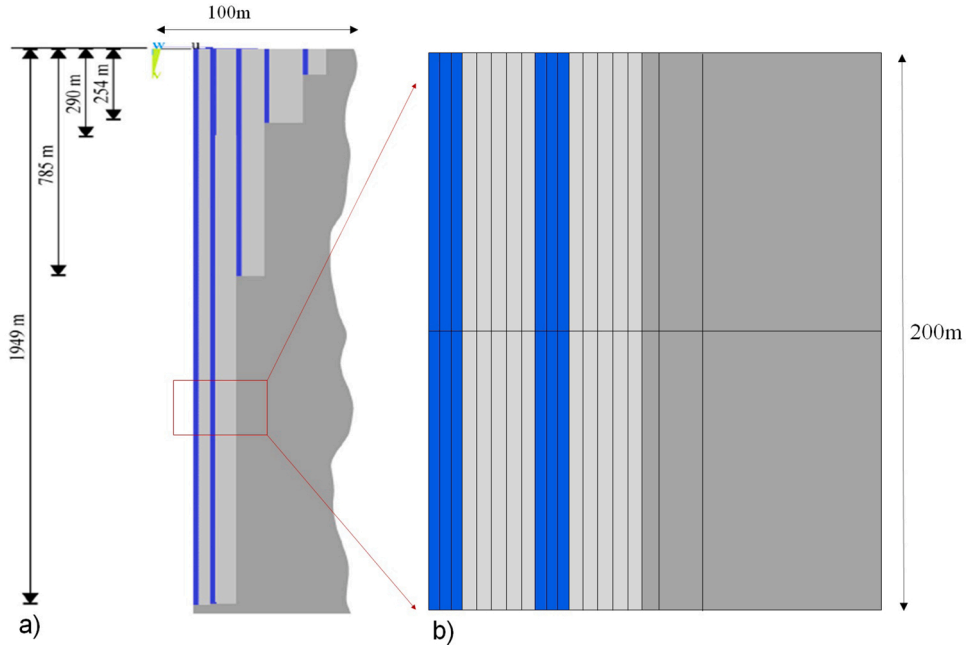

Fig. 13. (a) IDDP-1 well geometry as modelled by Kaldal et al. (2016) and (b) Illustration of the mesh in Casinteg's model, showed locally for a 200m well segment.

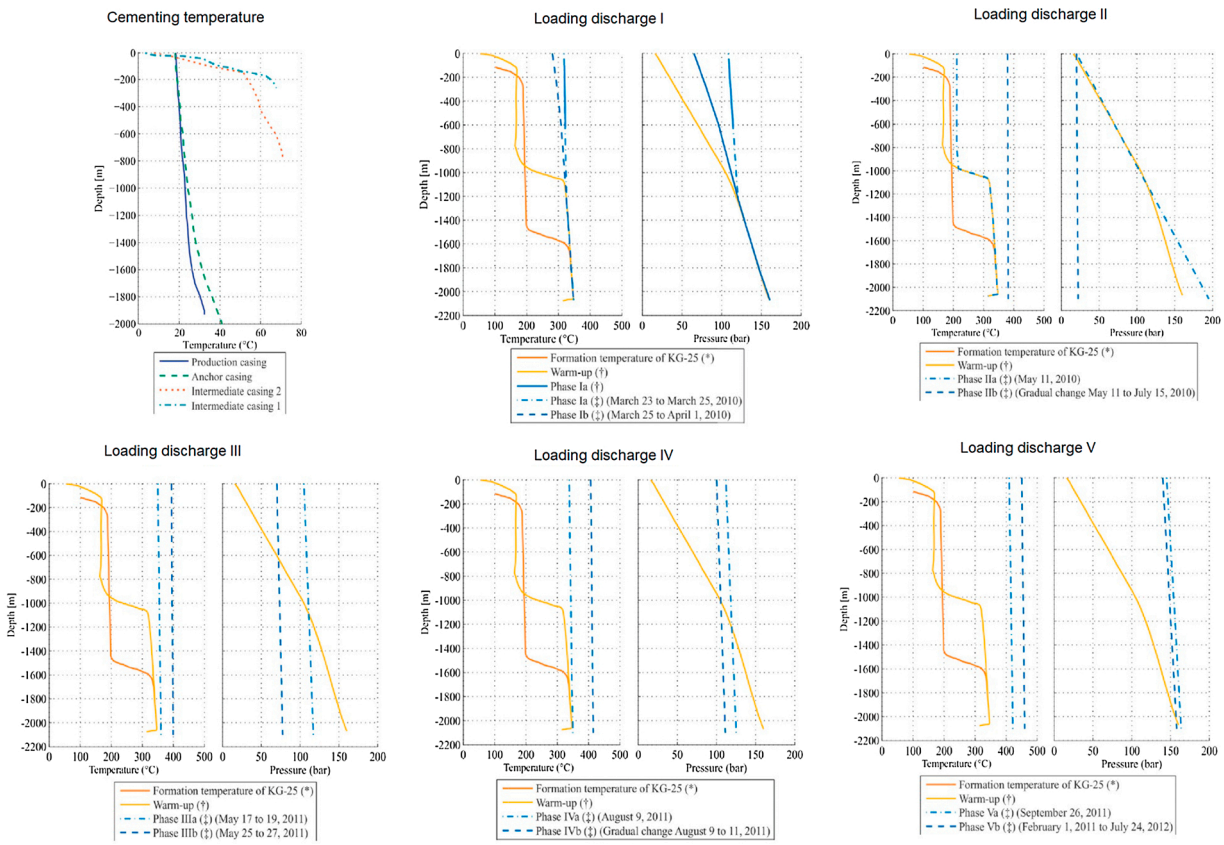

Fig. 14. Loading applied to the production casing of IDDP-1 well at different well periods (Kaldal et al., 2016).

different well life periods. It is to note that due to the lack of results for the discharge phase III documented in Kaldal et al. (2016), the results of solely warming-up and other four discharge phases were compared and discussed.

It can be seen that the results are very encouraging, showing a good agreement of the stress distribution in the production casing along the well depth between the Casinteg and Ansys simulations. The only major divergence is at the top of the well where the Ansys results tend toward zero. This is due to the fact that the wellhead geometry was modelled in the Ansys simulations, but not in the Casinteg ones. The presence of the wellhead allows the casing to slide and therefore minimizing the developed thermal stress in the casing segments close to the wellhead. In order to account for the wellhead effect in Casinteg, another simulation, in which the production casing segments close to the surface were allowed to slide using the Coulomb friction contact model, was performed. The simulation results were plotted in Fig. 17 along with the Ansys ones. In can be seen that the same tendency near the top of the well could finally be obtained. Moreover, the computational time of Casinteg simulations was under two minutes. This is a promising result, making Casinteg an attractive tool, not only for scientific investigations of the HT well physics but also for supporting an efficient casing system design.

5. Concluding remarks

Robust and cost-efficient casing systems for super HT applications are desired, allowing for harnessing the geothermal energy from high enthalpy reservoirs (temperature about 450–550 °C). However, this is a tough challenge to achieve due to the harsh design conditions (super hot and aggressive corrosion fluid) and due to the lack of standards regulating the casing system design practices for such super high operation temperatures. In order to provide a better understanding of the well physics, and thereafter supporting the robust casing design, a novel computational tool, Casinteg, was developed in HotCaSe project. The tool was intended to bridge the gap between the over-simplified analytic solutions and the complex finite element based commercial software. In this present paper, a short introduction to the constitutive models in Casinteg was presented, following by a preliminary verification study of these implemented models. The performance of the developed tool for modelling the full geothermal well under a complex load history was also investigated and demonstrated. From the present study, the following concluding remarks can be drawn:

- Casinteg is a simplified non-linear finite element based software, adapted for structural analyses of the global behaviour of wells, with an emphasis on geothermal wells. Casinteg allows for the transient analyses of heat transfer based on thermal conduction in the wells, and thereby studying the mechanical response of the casing systems under the applied thermal loads.
- Casinteg is based on the simplified 2D axisymmetric elements with reduced Degrees of Freedom to model the continuum materials in the well structure, i.e. casing pipe, cement and formation. In addition, the special contact element was implemented, allowing for the modelling of the interfacial behaviour (e.g. sliding and bonding) at multi-layer interfaces. Three material models, namely Thermo-Elastic, Thermo-Plastic, and Thermo-Plastic-Creep, were implemented in Casinteg to model the behaviour of casings strings, accounting for the temperature dependency of elastic properties (Young's modulus, Poisson's ratio), plasticity (yield stress and work hardening), and creep properties. The implemented models open up the flexibility in analysing the mechanical response of geothermal wells under thermal loading.
- For geothermal wells, steel casing pipes are generally expected to plastic yield under High Temperature loads. The present paper has shown that it is crucial to account for the Thermo-Plastic behavior during the warm-up, allowing for the strain-based design of the

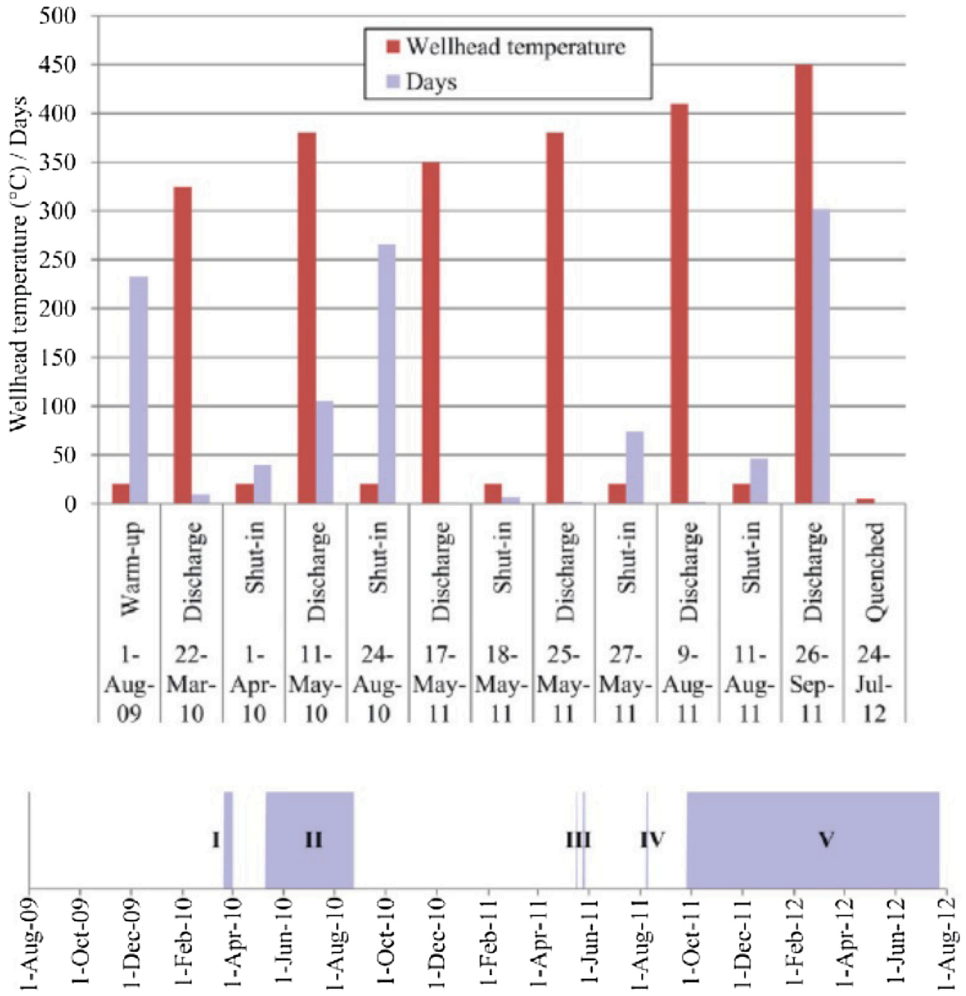

Fig. 15. Operation history and maximum wellhead temperature of each discharge phase of IDDP-1 (Kaldal et al., 2016).

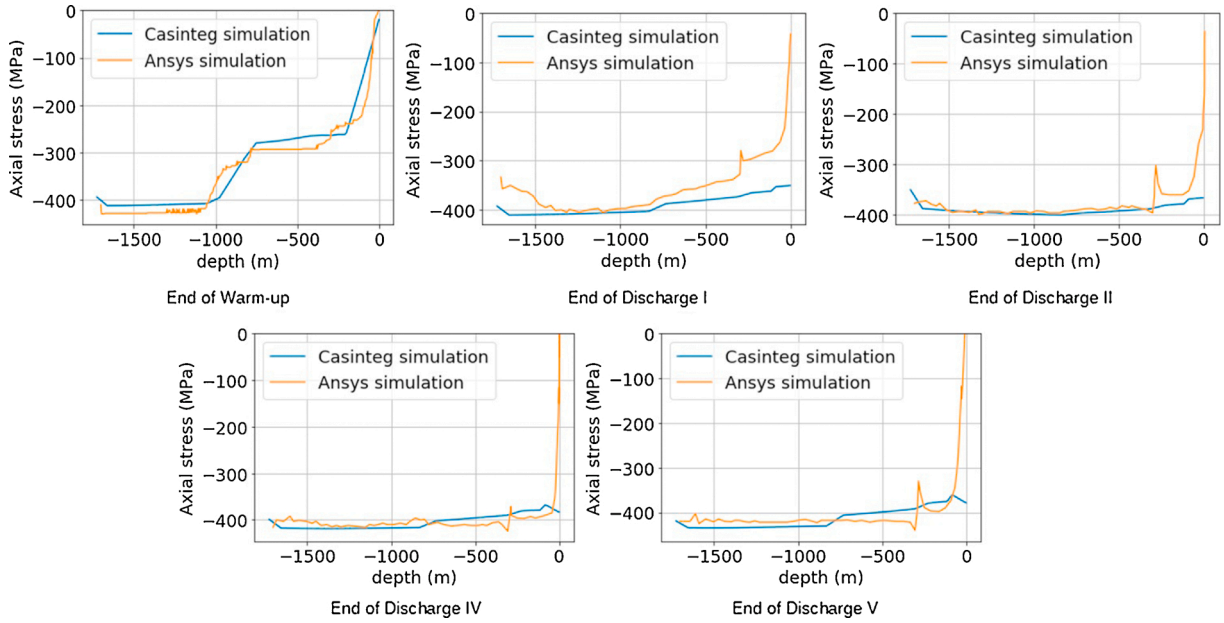

Fig. 16. Comparison of axial stress in the production casing at different times between Casinteg and Ansys models of IDDP-1 well. In these Casinteg simulations, the bonding contact behaviour between the production casing and cement was adopted.

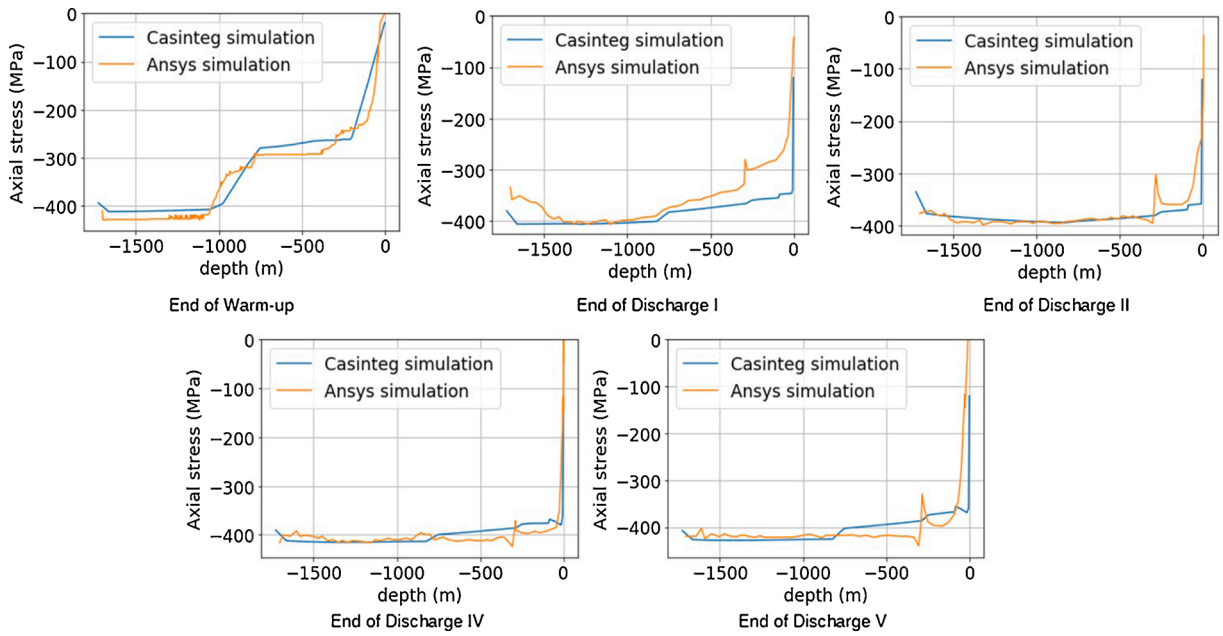

Fig. 17. Comparison of axial stress in the production casing at different times between Casinteg and Ansys models of IDDP-1 well. In these Casinteg simulations, the sliding contact behaviour between the production casing and cement was adopted.

casing. The creep behavior, which dictates the stress relaxation with time in the casing under constant strain, is of importance to be considered when dealing with cyclic loading, e.g. when the well is cooled down after long operation period. The stress relaxation at the constant operating temperature results in a higher tensile stress in the casing when cooled down. As a result, the creep behavior of casing cannot be neglected for a reliable design of geothermal wells, especially when dealing with super-HT application.

- The preliminary verification of the implemented constitutive models was carried out by benchmarking Casinteg with Abaqus software using 12m long models of multi-layers composite structures (i.e. casing string, cement sheath, and formation). The study showed a good agreement between Casinteg and Abaqus simulation results when modelling the heat transfer by conduction, and the structural response of casings under thermal loads. It depicted the reliability of the constitutive models implemented in Casinteg, ensuring the confidence in using the developed tool for geothermal casing designs.
- Low computation cost of Casinteg simulations is an asset for efficient global well analyses. With exactly the same models, it is about ten time faster to perform simulations in Casinteg than in Abaqus. The higher computation performance in Casinteg is mainly due to the reduced degree of freedoms of the implemented elements and the automatic differentiation methods made available in Julia. The computational efficiency of Casinteg can even be significantly increased by selecting appropriate mesh sizes. The implemented Casinteg's continuum elements are less mesh dependent in comparison with the conventional ones in the commercial software. Solution convergence for Casinteg simulations was obtained with a very high element aspect ratio.
- The performance of Casinteg for modelling of full geothermal wells of thousands meter depth was also demonstrated, based on IDDP-1 well case study. The stress evolution in the production casing along the well depth at different well events was analysed and compared with the Ansys simulation results by Kaldal et al. (2016). A perfectly one-to-one comparison was not possible due to the different nature of the two codes in modelling the involved materials behaviour, boundary conditions and loading. However, the preliminary results were encouraging, showing a good agreement of the obtained stresses in the production casing from both the Casinteg and Ansys models. In addition, with the optimal mesh size the computational time of Casinteg simulations was under two minutes. This is an attractive result, when comparing with the high computational cost for the similar simulations in the commercial FE-based software.
- There are still limitations in the current developed tool, and further developments are needed for reliable well analyses in Casinteg, as discussed in Section 2.3. Among which is the need to develop an advanced poro-mechanical material model to simulate cement behaviours at high temperature conditions, including the cement compaction due to pore collapse and the pore pressure build-up. In addition, the cement hydration effect, e.g. the volumetric change (shrinkage/swelling) and the hydration heat, would need a better model than the current version to be simulated. This will be investigated and discussed in the authors' further work. However, with its flexibility and efficiency, Casinteg could contribute to provide a better understanding of the geothermal well physics, bridging the gap in the current standard codes for designing robust casing systems.

Authors' contribution

Nguyen Hieu Hoang: Conceptualization, Methodology, Software, Investigation, Writing – Original Draft, Writing – Review & Editing, Project administration; Philippe Mainçon: Software, Writing – Original Draft; David Philippe: Validation, Visualization, Writing – Original Draft; Terence Coudert: Software, Writing – Review & Editing; Arve Bjørset: Supervision, Writing – Review & Editing; Sturla Sæther: Supervision, Writing – Review & Editing, Funding acquisition, Project administration.

Declaration of Competing Interest

The authors report no declarations of interest.

Acknowledgment

The authors would like to thank HotCaSe project (funded by Research Council of Norway with grant number NFR269399) for their financial support.

References

A. ANSI, T. API, 5C3, Technical Report, Technical Report on Equations and Calculations for Casing, Tubing, and Liner, 2008.

Axelsson, G., Gunnlaugsson, E., 2000. Background: geothermal utilization, management and monitoring. Long-Term Monitoring of High- and Low Enthalpy Fields Under Exploitation, pp. 3–10.

Benderitter, Y., Cormy, G., 1990. Possible Approach to Geothermal Research and Relative Costs, Small Geothermal Resources: A Guide to Development and Utilization. UNITAR, New York, pp. 59–69.

Bezanson, J., Edelman, A., Karpinski, S., Shah, V.B., 2017. Julia: a fresh approach to numerical computing. SIAM Rev. 59, 65–98.

Bois, A.-P., Garnier, A., Galdiolo, G., Laudet, J.-B., et al., 2012. Use of a mechanistic model to forecast cement-sheath integrity. SPE Drill. Complet. 27, 303–314.

Drilling, C.C. (DACC), November 2012. In Situ Heavy Oil Operations: An Industry Recommended Practice (IRP) for the Canadian Oil and Gas Industry IRP03, Technical Report, vol. 3, Enform Canada, Calgary, Canada.

Elders, W.A., Friðleifsson, G., 2010. The science program of the Iceland deep drilling project (IDDP): a study of supercritical geothermal resources. Proceedings of the World Geothermal Congress.

Friðleifsson, G., Pálsson, B., Albertsson, A.L., Stefánsson, B., Gunnlaugsson, E., Ketilsson, J., Gíslason, P., 2015. IDDP-1 drilled into Magma-world's first Magma-EGS system created. World Geothermal Congress 19–25.

Friðleifsson, Ó.G., Albertsson, A., Stefánsson, A., Şórólfsson, G., Mesfin, K.G., Sigurðsson, K., Sigurðsson, Ó., Gíslason, Ş., 2019. The Reykjanes DEEPEGS demonstration well-IDDP-2. European Geothermal Congress.

Gruben, G., Dillingh, B., Kaldal, G.S., Hoang, N.-H., Wollenweber, J., Rørvik, G., Thorbjornsson, I., Nyhus, B., 2021. Thermo-mechanical tensile testing of geothermal casing materials. Geothermics 89, 101944.

Hibbitt, H., Karlsson, B., Sorensen, P., 2012. Abaqus Theory Manual, Version 6.12, Pawtucket, Rhode Island, USA.

Hoang, N.-H., Lademo, O.-G., Sæther, S., Kampfer, G., Sørlie, C., 2020. Casing construction for supercritical geothermal power plant-HotCaSe. Proceedings of the World Geothermal Congress.

Hochstein, M., 1990. Classification and Assessment of Geothermal Resources, Small Geothermal Resources: A Guide to Development and Utilization. UNITAR, New York, pp. 31–57.

Holliday, G., 1969. Calculation of allowable maximum casing temperature to prevent tension failures in thermal wells. [preprint]. Prepr. ASME Petrol. Mech. Eng. Conf. (United States).

Kaldal, G.S., Jonsson, M.T., Palsson, H., Karlsdottir, S.N., 2015. Structural modeling of the casings in high temperature geothermal wells. Geothermics 55, 126–137.

Kaldal, G.S., Jonsson, M.T., Palsson, H., Karlsdottir, S.N., 2016. Structural modeling of the casings in the iddp-1 well: load history analysis. Geothermics 62, 1–11.

Kruszewski, M., Wittig, V., 2018. Review of failure modes in supercritical geothermal drilling projects. Geotherm. Energy 6, 28.

Muffler, P., Cataldi, R., 1978. Methods for regional assessment of geothermal resources. Geothermics 7, 53–89.

N.Z.S.N. 2403, Code of Practice for Deep Geothermal Wells, Technical Report, New Zealand Standards Council, 2015.

Ragnarsson, Á., Durst, P., Randeberg, E., Reinsch, T., Thorbjornsson, I., Wollenweber, J., Jong, W.d., Kampfer, G., Sigurdsson, Ó., Vercauteren, F., 2018. GeoWell-Innovative Materials and Designed for Long-Life High-Temperature Geothermal Wells. Urban Verlag Hamburg/Wien GmbH.

Rahman, S.S., Chilingarian, G.V., 1995. Casing Design-Theory and Practice, vol. 42. Elsevier.

Reinsch, T., Dobson, P., Asanuma, H., Huenges, E., Poletto, F., Sanjuan, B., 2017. Utilizing supercritical geothermal systems: a review of past ventures and ongoing research activities. Geotherm. Energy 5, 16.

Saint-Marc, J., Garnier, A., Bois, A.-P., et al. Initial state of stress: the key to achieving long-term cement-sheath integrity. In: SPE Annual Technical Conference and Exhibition, Society of Petroleum Engineers.

Snyder, R.E., 1979. Casing failure modes in geothermal wells. Geotherm. Resour. Council Trans. 3, 667–670.

Southon, J.N., 2005. Geothermal well design, construction and failures. Proceedings of the World Geothermal Congress 24–29.

Thorbjornsson, I.O., 2016. Material challenges for high temperature geothermal wells: a short description of two new European projects on geothermal wells. Seminar Materials Challenges in Geothermal Utilization.

Zienkiewicz, O.C., Taylor, R.L., 2005. The Finite Element Method for Solid and Structural Mechanics. Elsevier.